International Journal of Innovative Research in Computer Science and Technology (IJIRCST)
ISSN(Online): 2347-5552, Volume-13, Issue-2, March 2025
https:/doi.org/10.55524/ijircst.2025.13.2.7
Article ID IJIRD-1380, Pages 42-53
www.ijircst.org

Adjoint-Based Optimization for Enhanced Aerodynamic Performance Using Multi-Parameterization Techniques

Sheharyar Nasir[1], Shumail Sahibzada[2], and Farrukh Sher Malik[3]

[1] Doctoral Student, Department of Aerospace Engineering, University of Kansas, Lawrence, Kansas, USA
[2] MSc Data Analytics, Park University, Parkville, Missouri, USA
[3] MSc Information Technology, Park University, Parkville, Missouri, USA

Correspondence should be addressed to Sheharyar Nasir; Sheharyarnasir@ku.edu

Received: 9 February 2025 Revised: 22 February 2025 Accepted: 9 March 2025

ABSTRACT- Airfoil shape optimization is imperative for enhancing the aerodynamic performance of the aircraft. In the shape optimization process, geometry parameterization holds a pivotal role; directly influencing its robustness and efficiency. In this study, Adjoint-based shape optimization of the airfoil RAE-2822 was performed at transonic Mach while employing two parameterization methods – Hicks-Henne and FFD. The prime objective is to compare the efficiency of parameterization techniques and form comparison metrics based on their five fundamental characteristics - Parsimony, Intuitiveness, Orthogonality, Completeness, and Flawlessness. The optimization framework is composed of an open-source CFD solver, a discrete adjoint solver for gradient evaluation, and a gradient-based optimizer (SLSQP) for optimization. While using both techniques, the process resulted in a total drag reduction of around sixty-seven percent and an increase in aerodynamic efficiency by nearly three times. However, in the comparison metrics, it was seen that FFD outperforms Hicks-Henne exhibiting better properties in terms of parsimony and intuitiveness.

KEYWORDS- Adjoint, Optimization, Aerodynamic Performance, Multi-Parameterization Techniques

I. INTRODUCTION

Aerodynamic design optimization has been the subject of extensive investigation in the aviation industry and has become an indispensable component of the aircraft design process. Aerodynamic shape optimization allows the aircraft to achieve ambitious targets in terms of efficiency and, in turn, be economically and environmentally viable. Earlier this, process could be performed through experimentation, which is a resource-intensive process both computationally and cost-wise. With rapid evolvement in computational physics, the evaluation of alternative designs by numerical simulations has become practical [1] [2] [3] [4] [5] [6]. In the numerical-based approaches, different schemes have been utilized to achieve the optimization goal with less computational effort and more fidelity [7] [8] [9] [10]. However, in the numerical-based approach, for high-fidelity aerodynamic shape optimization, the CFD solver coupled with the adjoint solver has proven to be the most feasible and efficient method [11] [12] [13] [14] [15].

The adjoint method was developed by Jameson [16] and was applied to aerodynamic optimization [17] [18]. Since then, various researchers have implemented the methodology in numerous aerodynamic shape optimization problems to both two-dimensional and three-dimensional problems [19] [20] [21] [22] [23] [24] [25] [26] [27] [28]. The computational cost involved in the solution of adjoint equations is comparable to one flow solution and yield gradients with respect to all design variables, which makes the method far more efficient than the finite-difference or the complex-step method. EJ Neilson and WK Anderson [20]implemented the adjoint technique into an unstructured Navier-stokes solver[20]. Telidetzki et al [21]applied adjoint based optimization technique for the design case of NACA 0012 and used Jetstream as a flow solver[21]. Reuther et al [23] performed adjoint based optimization to conduct an aerodynamic shape optimization of complex aircraft configuration. Anderson and Venkatakrishnan [24]derived continuous adjoint equations for the incompressible Navier Stokes (N-S) equations. Elliot et al [29] implemented the discrete adjoint equations for compressible Navier-stokes (N-S) equations and also included the turbulence effects. Bonhaus and Anderson [25] performed adjoint based optimization while using RANS equation with Spalart-Allmaras (SA) turbulence model. Palacios et al[30] applied continuous adjoint method to the Navier-stokes (N-S) equations. Yayun shi et al [31]applied discrete adjoint based optimization technique coupled with RANS solver on the aerodynamic shape optimization of natural laminar-flow airfoil. Mangano et al [32]applied multipoint adjoint based optimization to the design of airfoil and wing at supersonic, subsonic and off-design conditions.

However, the challenges persist in adjoint based approach including efficient design space exploration, effective control of a geometry, and the solution of a global optima. The flexibility of exploring the design space, direct control over geometry parameters, and robustness of the optimization process is largely dependent on shape parameterization [31][32][33][34][35][36]. Thus the choice of parameterization method is crucial for the optimization[37].

Parameterization formulates a given geometry into a mathematical form and the shape is defined through control points, which makes the optimization process

efficient, and less time consuming. An effective and efficient parameterization method is characterized by its five fundamental properties; parsimony, intuitiveness, orthogonality, completeness and flawlessness [38]. Class-shape transformation (CST)[39], polynomials and splines[40] fall in the category of constructive parameterization method. In constructive methods, difficulties may arise while parametrizing the sharp edges or unsmooth profiles[35]. The Deformative methods such as Hicks-Henne (HH) bump functions[41], basis vector [42]and Free-form deformation method[43][44] takes the existing geometry and deform it to create a new shape, and the sharp edges and unsmooth profiles are parameterized with ease[35]. Hicks-Henne and FFD methods offer more global control than CST, Parsec and Ferguson's, etc[38], and explore the design space more efficiently. Also because of the multiple advantages of these methods, it is widely used in aerodynamic shape optimization (2-D and 3D) configurations [31,][32][33][34][35][36]. Leifsson et al implemented a PARSEC parameterization technique [45] and used twelve parameters for defining the control points[45] over RAE-2822 and NACA 0012 geometries. Samareh et al[42] studies revealed that efficient parameterization process is characterized by five attributes that includes providing geometry consistent changes, accurate sensitivity derivatives, and a compact and effective set of design variables. Amoignon et al [46] carried out a comparison of two parameterization techniques, FFD and Radial Basis Function (RBF), and optimized RAE 2822 and NACA 0012 airfoils while using sequential quadratic programming (SQP) as an optimizer and unstructured flow solver EDGE. A drag reduction of 361.2 drag counts and 68 drag counts was achieved respectively using FFD[46] whereas with RBF technique, a drag reduction of 78 drag counts was achieved for the RAE 2822[46]. Sripawadkul et al [38] formed comparison metrics for five parameterization techniques – (CST, Hicks Henne, Bspline, Ferguson's curve and PARSEC) on the basis of five desirable characteristics including completeness, flawlessness and orthogonality. Carrier et al[22] applied Bezier curve parameterization technique to parameterize the NACA 0012 and RAE 2822, and was able to achieve a drag reduction of 387.1 drag counts and 91.4 drag counts for NACA 0012 and RAE 2822 respectively. Masters et al. employed various airfoil parameterization methods belonging to the two categories and studied how these methods influence the optimized airfoil shape [35]. Mangano et al[32] applied FFD parameterization technique with discrete adjoint solver for the optimization of both the airfoil and wing.

In the literature review section, contributions of various authors have been presented. It is quite evident that no author has undertaken the study to investigate the fidelity of shape parameterization techniques (Hicks-Henne and Free Form Deformation) based on five desirable characteristics (Parsimony, Intuitiveness, Flawlessness, Orthogonality, and Completeness) using adjoint-based optimization. Moreover, the comparison metrics that were formed by Sripawadkul et al [38] did not include FFD technique in his research. This study also aims to address this gap and form comparison metrics based on the five desirable properties for both parameterization techniques.

II. METHODOLOGY

In the present study, an adjoint-based aerodynamic shape optimization of the RAE-2822 airfoil was performed under transonic conditions (Mach 0.8). The primary objective was to evaluate the influence of two distinct parameterization techniques—Hicks-Henne (HH) and Free-Form Deformation (FFD)—on the optimized geometry and aerodynamic performance of the airfoil. These two methods were selected for their differing approaches to geometry manipulation and their potential impact on optimization efficiency.

The numerical modeling and fluid flow analysis were conducted using SU2, an open-source computational fluid dynamics (CFD) solver known for its robust capabilities in handling aerodynamic simulations. SU2 was employed to solve the Reynolds-averaged Navier-Stokes (RANS) equations, capturing the aerodynamic behavior of the airfoil. For gradient evaluation, the discrete adjoint method was implemented, allowing for efficient computation of the sensitivity of the aerodynamic performance with respect to the design variables. To perform the optimization, a gradient-based optimizer, Sequential Least Squares Quadratic Programming (SLSQP), was employed, which iteratively adjusts the design variables to minimize the drag and maximize the aerodynamic efficiency of the airfoil.

A critical aspect of this study was the deviation analysis, which involved comparing the optimized geometries obtained from both Hicks-Henne and FFD parameterizations with a reference geometry from the literature. This analysis aimed to quantify the differences between the optimized shapes and evaluate the accuracy of the optimization process. The deviation analysis not only serves as a validation step for the framework but also provides insight into the effectiveness of each parameterization method in achieving the desired aerodynamic characteristics. By examining these geometrical deviations, it was possible to assess the robustness of the optimization methods and their ability to accurately replicate known optimal geometries.

Furthermore, a comprehensive comparison metric was developed to evaluate the performance of the two parameterization techniques across five key characteristics: Parsimony, Intuitiveness, Orthogonality, Completeness, and Flawlessness. These metrics provide a holistic view of the strengths and weaknesses of each method, guiding the selection of the most suitable parameterization approach for aerodynamic shape optimization tasks. The framework and methodology employed in this study, including the CFD setup, optimization process, and comparison metrics, is illustrated in Figure 1.

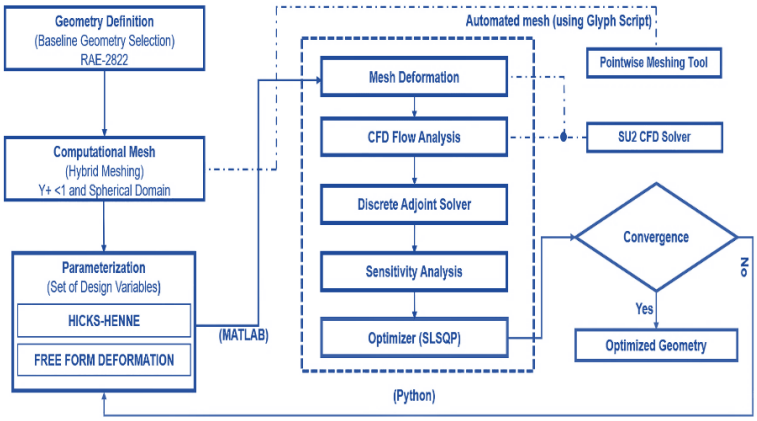

Figure 1: Aerodynamic Shape Optimization Flowchart

Figure 1 presents the flowchart of the methodology used for aerodynamic shape optimization. The process begins with selecting the baseline geometry, followed by computational meshing and parameterization. Mesh deformation is then applied, leading to CFD analysis, Adjoint solver calculations, and the optimization technique. The process concludes once the optimized geometry is achieved.

A. Hicks-Henne Bump Functions (HH)

In the Hicks-Henne method, a linear combination of a set of n basis functions (defined between 0 and 1) and base airfoil information are used to determine the final airfoil shape. The airfoil surfaces are defined by

$$y = y_{baseline} + \sum_{i=1}^{m} \theta_i f_i(x), \qquad 0 \le x \le 1$$

$y_{baseline}$ refers to the baseline airfoil coordinates, θ_i $(i = 1, \dots, m)$ are the design variables and their product with the basic functions $f_i(x)$ control the shape of the airfoil. The basic functions $f_i(x)$ are sine functions and are defined through:

$$f_i(x) = \left[\sin(\pi x^{\frac{\ln 0.5}{\ln h_i}})\right]^{t_i}$$

In equation 3-13, t_i the parameter is used to control the width of the bump whereas h_i refers to the location of the maximum amplitude of the bump function which is further defined by -
for $i = 0, \dots, n, l = 0, \dots, l$.
The two-dimensional Bezier surface is given by:

$$\Psi(u,v) = \sum_{j=0}^{l} \sum_{i=0}^{n} B_i^n(u)\ B_j^l(\mathrm{v}) P_{ij}$$

$$u(x) = \left(\frac{x - x_{min}}{x_{max} - x_{min}}\right),\ v(z) = \left(\frac{z - z_{min}}{z_{max} - z_{min}}\right)$$

The deformation of the initial airfoil with respect to the design variables is defined as

$$= \sum_{j=0}^{l} \sum_{i=0}^{n} B_i^n(u(x_{initial})\ B_j^l(v(y_{initial}) P_{ij}$$

In this study, control point movement was restricted in the z-direction, 2nd order FFD continuity equation was used for the surface continuity at the intersection with the FFD, and FFD tolerance was set at the value of 1^{e-10}. FFD of

Where u,v ϵ [0,1] and B_i^n are Bernstein polynomials.
The undeformed domain is normalized to the unit dimension by the transformation.

$$h_i = \frac{1}{2}\left[1 - \cos\left(\frac{i\pi}{m+1}\right)\right], \qquad i = 1, \dots, m$$

In the current study, multiple sine functions (also referred to as design variables) ranging from 4 to 36 were placed on both the upper and lower surfaces of the airfoil. Following the preferable approach, the bumps were placed equally and the width was set at the value of 3.

B. Free-Form Deformation (FFD)

The parametric space of the FFD box is defined through a parallelepiped lattice of control points which are generated through NURBS, B-splines or Bezier curves [47] and each choice has its own impact on the FFD characteristics.. Thus when the control points are modified or the lattice is deformed, the object inside the box also deforms in a similar fashion hence creating a new geometry[43]. The lattice of control points is defined through the degree of polynomial.
In FFD, a deformable domain of a rectangular lattice of order $(m+1)$ x $(n+1)$ is created and design variables, P_{ij}, are uniformly placed around an initial airfoil. The initial positions of the control points are defined by:

$$P_{ij}^{initial} = \left(x_{min} + \frac{i}{m}(x_{max} - x_{min}), y_{min} + \frac{j}{n}(y_{max} - y_{min})\right) X$$

multiple orders (2x1, 4x1, 6x1, 8x1, and 10x1) were implemented, however, best results with a minimum number of design iterations were found using the lattice space of 4x1.

C. Flow Solver

The flow field analysis around the airfoil was governed through RANS equations using SU2, which is a finite volume-based solver and has tremendous application in aerospace industry. Jameson-Schmidt-Turkel (JST) scheme is utilized for spatial discretization whereas, for time marching, an implicit Euler scheme is used.

Monotone Upstream centered Schemes for Conservation Laws (MUSCL) approach was used in conjunction with gradients limiter –VENKATAKRISHNAN to achieve second-order accuracy. To accelerate the convergence of the numerical solutions, the V-Cycle multi-grid of 2nd level was utilized in the flow solution. SST-K omega, which is a 2-equation turbulence model was used to achieve accurate solutions in the far field and near wall regions. On the boundary of the domain and at the wall, the far-field boundary condition and no-slip condition were set respectively.
RANS equation is mathematically defined by-

$$\int_{\Omega i} \frac{\partial U}{\partial t}\, d\Omega + \sum_{j\in N(i)} (\bar{F}_{cij} + \bar{F}_{vij})\Delta S_{ij} - Q|\Omega i| = \int_{\Omega i} \frac{\partial U}{\partial t}\, d\Omega + R_i(U) = 0,$$

Where U is the vector of primitive variables, $\bar{F}_{cij}$ and $\bar{F}_{vij}$ are convective and viscous fluxes and Q is a source term.

D. Adjoint Method

Adjoint method is used for the computation of the gradient of objective function with respect to design variables and requires a single CFD solution for the computation of gradient (of objective function and constraints with respect to all the design variables), making the method far more efficient than finite-difference and complex step methods. In this study, discrete adjoint solver has been utilized coupled with JST and Euler implicit schemes for the spatial and time discretization respectively. Mathematically the adjoint equations are defined by

$$f = f(x, w)$$
$$R(x, w) = 0$$

Above equation is the residual form of the Navier-stokes equation.
Using chain rule-

$$\frac{df}{dx} = \frac{\partial f}{\partial x} + \frac{\partial f}{\partial w}\frac{dw}{dx}$$
$$\frac{dR}{dx} = \frac{\partial R}{\partial x} + \frac{\partial R}{\partial w}\frac{dw}{dx} = 0$$

This can be rearranged to get the linear system

$$\frac{\partial R}{\partial w}\frac{dw}{dx} = -\frac{\partial R}{\partial w}$$
$$\frac{df}{dx} = \frac{\partial f}{\partial x} - \frac{\partial f}{\partial w}\left(\frac{dR}{dw}\right)^{-1}\frac{dR}{dx}$$
$$\frac{dR}{dw}^{T}\ \varphi = \frac{\partial f}{\partial w}$$

The above equation is an adjoint equation.

Substituting the adjoint vector into the second last equation, we get

$$\frac{df}{dx} = \frac{\partial f}{\partial x} - \varphi^{T}\frac{\partial R}{\partial x}$$

E. Mesh Deformation

After geometry perturbation through parameterization, the volume mesh needs to be deformed. In this study for the mesh deformation, inverse volume method was utilized which is based on equations of linear elasticity. In this method, the computational mesh is treated as an elastic solid model and the modulus of elasticity for each mesh cell is approximated to be inversely proportional to the cell volume. This method helps to preserve the mesh quality in the boundary layer region and regions of high resolution. The linear elasticity equations are mathematically defined as-

$$\frac{\partial V^2}{\partial t^2} - \nabla\sigma = f\ in\ \Omega, t > 0$$

Where f is a body force and σ is referred as stress tensor which is given in terms of strain tensor, ϵ, by the following relations

$\sigma = \lambda Tr\,(\epsilon)\,\mathrm{I} + 2\mu\,\epsilon$, $\epsilon = \frac{1}{2}(\nabla \mathrm{u} + \nabla \mathrm{u}^{\mathrm{T}}), \lambda = \frac{vE}{(1+v)(1-2v)}$, $\mu = \frac{\mathrm{E}}{2(1+\mathrm{v})}$,

F. Optimization

In gradient-based optimization, the minimization of the objective function with respect to the control points is done using the gradient information acquired through sensitivity analysis. These gradients evaluated through adjoint guide the design towards an optimum design. Since gradient-based optimization is an iterative process so for each new design, a new set of control points are generated and the objective or constraint functions are evaluated with respect to this new set of design variables. This process repeats till the Karush-Kuhn-Tucker (KKT) optimality condition is satisfied. There are various gradient-based optimizers, however, in the present study, SLSQP (in a Python-based package) has been utilized based on its ability to solve non-linear constrained problems and has been tested efficiently for optimization problems with large number of constraints and design variables.
A general optimization problem can be defined according to equation 4-1:

$$Minimize\ f(X), w.r.t\ X$$
$$subject\ to\ g_j\,(X) \le 0, j \in [1, \dots, m]$$
$$h_k(X) = 0, k \in [1, \dots, l]$$

Whereas X is the set of nX control points or design variables, f is the objective function that is to be minimized, g_j and h_k are the inequality and equality constraint functions respectively that must satisfy. In this study, the optimization is achieved through gradient-based optimizer SLSQP.

G. Sequential Least Square Quadratic Programming (SLSQP)

SLSQP is a second order optimization algorithm, is used to minimize a function that is based on several design variables and has any combination of inequality or equality constraints. SLSQP is best suited for the optimization problems in which objective function and constraints are twice continuously differentiable. This method is originally developed by Dieter Kraft. It uses Han-Powell quasi-Newton method with a BFGS update of the B-matrix and L1-test function in the step length algorithm. The optimizer uses a slightly modified version of Lawson and Hanson's non-linear least-squares solver (NNLS).
Mathematically, it can be written as:

$$L(x, \lambda) = f(x) + \lambda^{T} g(x)$$

$$\nabla L(x,\lambda) = \begin{bmatrix} \nabla f(x) + J_g^T(x)\lambda \\ g(x) \end{bmatrix} = 0$$

Newton method used for the solution of above non-linear system can be written as:

$$x_{n+1} = x_n - \frac{f(x_n)}{f'(x_n)}$$

It can be rewritten as:

$$\bar{x}_{n+1} = \bar{x}_n - \frac{\bar{f}(x_n)}{\bar{f}'(x_n)}$$

Taking Jacobian of the gradient of Lagrangian with respect to x gives:

$$B(x,\lambda) = H_f(x) + \sum_{k=1}^{m} \lambda_k H_{g,k}(x)$$

$$J_g(x)$$

Re-arranging equation and bringing basic equation of matrices in comparison gives:

$$J_{\nabla L}\delta\bar{x}_n = -\overline{\nabla L}(x_n,\lambda)$$

$$A\,X = B$$

where, $\delta\bar{x}_n = \bar{x}_{n+1} - \bar{x}_n$

Solution of above equation gives us $\delta\bar{x}_n$ which can be used in combination of initial guess to find $\overline{x}_{n+1}$ Newton's iteration continues till the convergence criteria is met.

- Case Study 1- Initially, for validation of the optimization framework, a benchmark case has been considered in the paper. The case belongs to the viscid drag minimization of the RAE-2822 airfoil in transonic flow. The freestream mach number is 0.734 and the Reynold's number, Re, is $6.5.10^6$. Multiple constraints were imposed including lift coefficient (which should be 0.824), pitch moment coefficient must not be less than -0.092, and the airfoil area must be greater than or equal to the baseline airfoil area. The optimization problem is stated as

$$Minimize: C_d$$
$$Subject\ to: C_l = 0.824$$

$C_m \geq$ -0.092

$S \geq S_O$

where C_l, C_d and C_m are lift coefficient, drag coefficient, and moment coefficient respectively. S and S_O are the areas of the optimized and baseline geometry.

- Case Study 2- In this study, an RAE-2822 airfoil was optimized for a hypothetical fighter aircraft (as shown in Figure 2) at subsonic cruise conditions. The problem was viscid drag minimization case in a transonic flow with a lift coefficient constrained to 0.3867, airfoil angle of attack was also treated as an additional design variable to achieve the desired lift, and the airfoil area must be greater than or equal to the airfoil area (of NACA 64-204 airfoil which is generally used in fighter aircraft. The freestream Mach number was 0.80, and Reynold's number, Re, was 6.08 $x\ 10^6$. The free stream Mach number, pressure, and temperature were set based on the literature as fighter aircraft generally cruise at 0.80 Mach at 36000 ft altitude [48]. The angle of attack was set up as an additional design variable to satisfy the lift constraint. The few key parameters of the aircraft are summarized in Figure 2 along with the projection views.

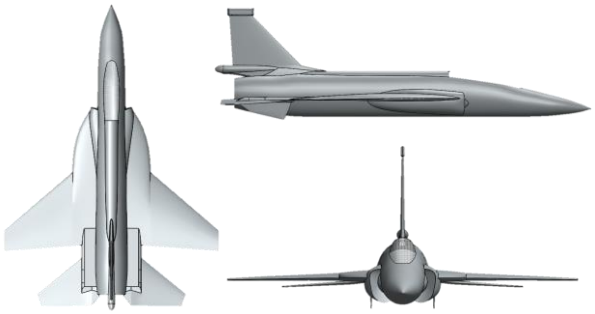

Parameters	Values
Gross Weight	22000 lbf
Wing Sweep	43.4°
Wing Aspect Ratio	3.14
Wing Dihedral	0°
C_{Lc} Aircraft	0.3306
C_{Lw} Wing	0.3480
C_l Airfoil *	0.3867

Figure 2: Projection views of the aircraft and its key attributes.

The optimization problem is defined by:

$$Minimize: C_d$$
$$Subject\ to: C_l = 0.3867$$

$S \geq S_O$.

H. Computational Mesh

For case study 1, an O-grid structured mesh was generated using the hyperbolic extrusion method. The computational domain consists of a no-slip airfoil surface and is bounded by a far-field at a distance of 50 chord lengths from the airfoil. The table illustrates that coarse mesh has a grid size of 200x138, where 200 grid points were distributed on the airfoil (100 points equally on upper and lower surfaces) and 138 grid points along y. Off-wall spacing of 1 x 10^{-5} was set to achieve y^+value below 1.0. Four levels of mesh were generated to establish grid convergence while keeping the grid topology the same. The refined meshes were generated by multiplying the grid size by a factor of 2. The key attributes of these meshes are summarized in Table 1.

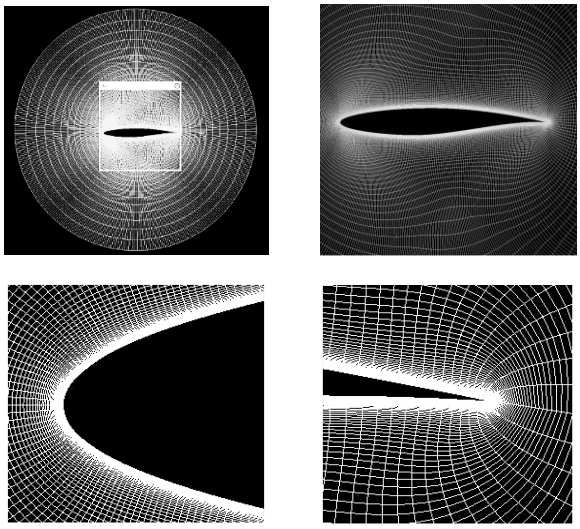

Figure 3: Computational mesh view – in far field, local region, leading edge and the trailing edge

Figure 3 illustrates the overall mesh topology used for meshing the geometry near the leading edge, trailing edge, and in the far field. The mesh is refined near the wall, as shown in Figure 3. RANS-based compressible flow analysis was performed on each mesh and the values of coefficients of lift and drag were evaluated. The values of the lift coefficient were almost similar in each case; however, minor deviations were found in the values of drag coefficients.

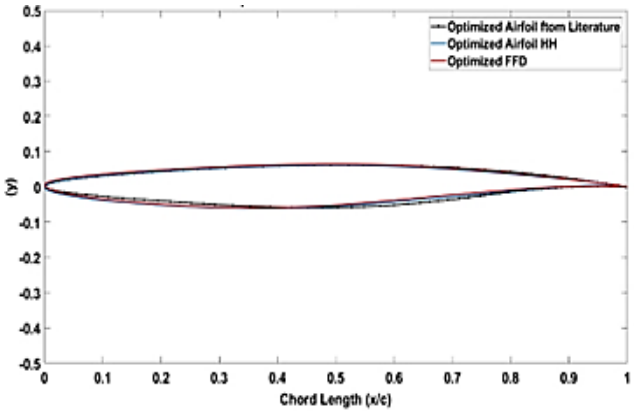

Figure 4: Framework Validation Results – Comparison of optimized geometries

Table 1: Key attributes of the computational mesh

Mesh Level	Off-wall Spacing	Grid Size	Mesh cells
Coarse	$1\ x\ 10^{-5}$	200 x 138	27600
Medium	$7.2\ x\ 10^{-6}$	400 x 141	56800
Fine	$5.0\ x\ 10^{-6}$	600 x 145	87000
Superfine	$3.5\ x\ 10^{-6}$	800 x 149	119200

The percentage error found in the values of the drag coefficient is shown in Table 2. The error was below 1 % in the case of medium-level mesh and was less resource-intensive, thus, it was used in both case studies 1 and 2.

Table 2: Grid Convergence study – Case study 1

Mesh Level	C_l	C_d	**Percentage error in C_d**
Coarse	0.8239	202.03	-
Medium	0.8240	195.18	3.39 %
Fine	0.8240	194.84	0.17 %
Superfine	0.8240	194.65	0.09

III. RESULTS AND DISCUSSION

A. Case Study 1

To establish the validation of the overall framework, a benchmark optimization problem (which is case study 1) was chosen. The geometry was parameterized using FFD and Hicks-Henne, and the results were compared against the ones already established in the literature [45]. Since the optimized geometries are very similar in comparison to the published work, thus for the sake of convenience, the pressure distribution achieved in the case of FFD parameterization is only shown and compared against the published work. The optimized geometries were also compared in terms of mean deviation, maximum deviation, and standard deviation through deviation analysis[49]. Figure 4 and Figure 5 compare the optimized geometries and pressure coefficient graphs with the model and data from the literature, validating our optimization setup.

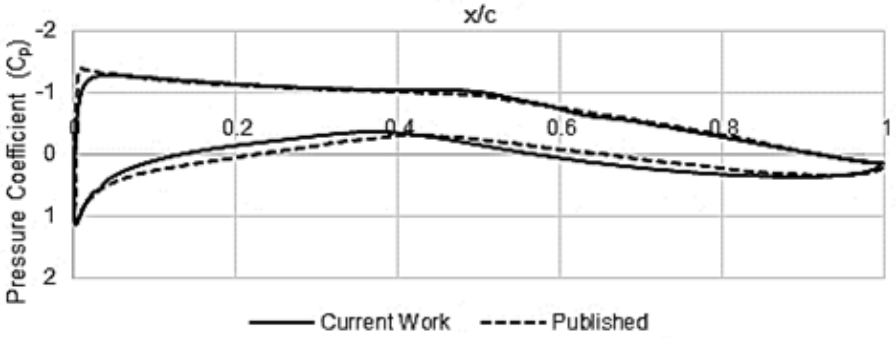

Figure 5: Framework Validation Results – Comparison of Pressure Coefficients

The validation results are summarized in table 3:

Table 3: Framework Validation Results - Comparison of values of C_l, C_d and $Area$

Optimized Geometry [9]	C_l	C_d	Airfoil Area	Percentage Error C_d
Literature	0.8240	0.01195	0.07784 m^2	-
Hicks-Henne	0.8240	0.01201	0.07784 m^2	0.5 %
FFD	0.8240	0.01210	0.07784 m^2	1.2 %

The deviation analysis was performed to compute the deviations between the surfaces in terms of key variables standard deviation, mean deviation, and maximum deviation. The deviation metrics are summarized in table 4 as:

Table 4: Deviation metrics

Parameters	Hicks-Henne	FFD
Maximum Deviation	0.2025 mm	0.1259 mm
Standard Deviation	0.0564 mm	0.0317 mm
Mean Deviation	0.0866 mm	0.592 mm

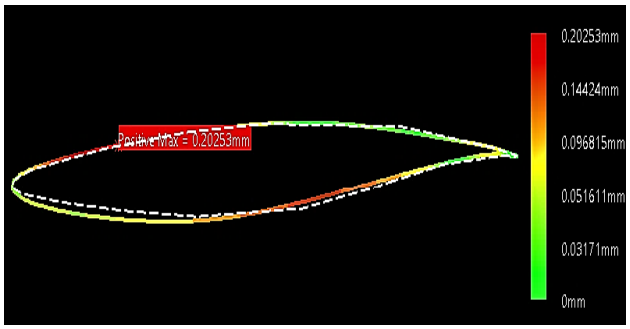

Figure 6: Deviation analysis between optimized geometries (HH and Literature)

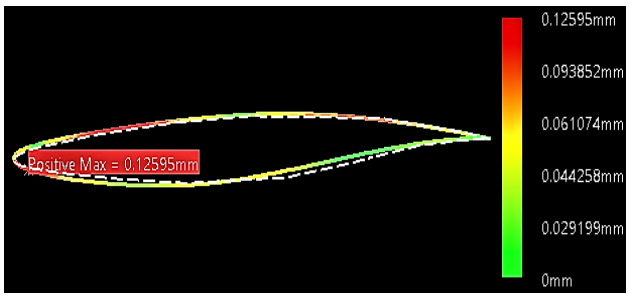

Figure 8: Deviation Analysis between optimized geometries (FFD and Literature)

Figure 6 and Figure 7 illustrate the deviation of the optimized geometry from the model sourced from the literature (for validation). These figures highlight regions of maximum and minimum deviation, showing that the deviation values fall within an acceptable range. From the deviation analysis and the corresponding statistical results, it is quite evident that the optimized geometries nearly fit exactly on the optimized airfoil found in the literature, which further strengthens the validation of the framework.

B. Case Study 2-

In case study 2, the airfoil was optimized for the hypothetical aircraft at the subsonic cruise condition as stated in the earlier section. Geometry was parameterized using both techniques and was optimized to explore the fundamental characteristics of the methods. The baseline geometry and the Cp distribution plot are shown in Figure 8.

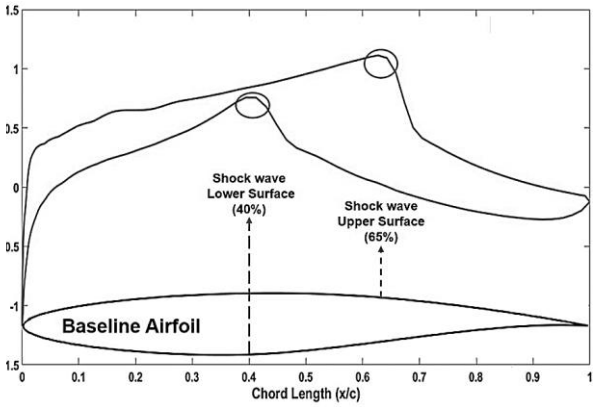

Figure 7: Cp Distribution of a baseline airfoil at Mach 0.80 and at 36000 ft altitude.

From the Cp distribution plot, it was seen that at forty percent of the chord length along the lower surface and at sixty-five percent of the chord length along the upper surface, a sharp rise in pressure and temperature gradients was observed. The velocity and Mach dropped sharply at these locations; these flow features indicate the presence of a shock wave at these locations. These shock waves had given rise to the total drag of the airfoil and had led to a significant decrement in the aerodynamic efficiency of the airfoil at this flow condition.

The aerodynamic characteristic of the baseline airfoil is summarized in table 5 as:

Table 5: Aerodynamic characteristics of the baseline airfoil at Mach 0.8

Parameters	Values
Lift Coefficient C_l	0.3867
Drag Coefficient C_d	0.0246
Aerodynamic Efficiency	17.85
Airfoil Area	0.07784 m^2

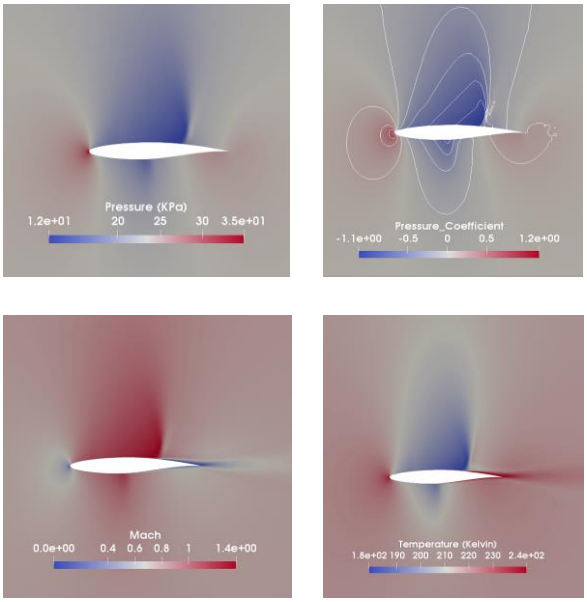

Figure 9: Pressure, Cp, Temp, Mach Contours for the baseline geometry.

Figure 9 shows various flow properties contours for the baseline geometry. In all the contours, a sharp gradient could be seen indicating the presence of shock on the upper and lower surfaces of the airfoil.

Figure 10 and Figure 11 present the Cp distribution of both the optimized geometries and the baseline. Figure 10 displays the Cp distribution for the optimized geometry using the HH method, while Figure 11 shows the Cp distribution for the geometry optimized with the FFD method.

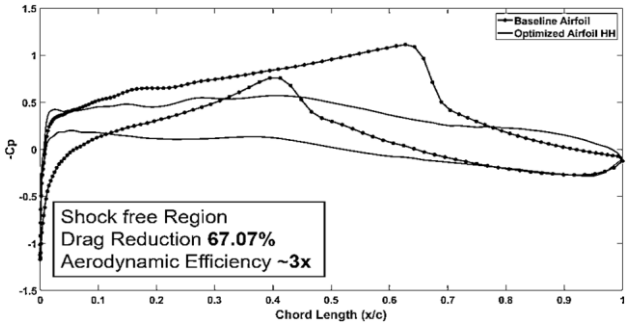

Figure 10: Comparison of Cp Distribution – Baseline Vs Optimized geometry (using Hicks-Henne)

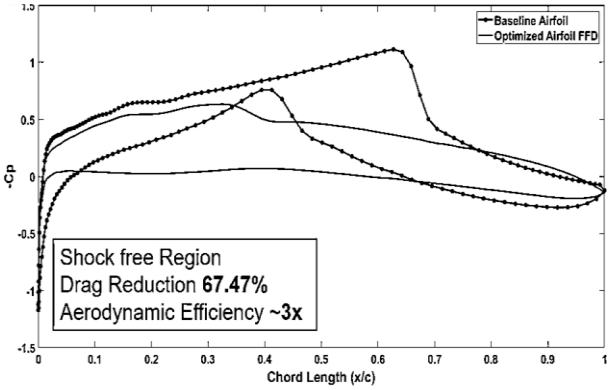

Figure 11: Comparison of Cp Distribution – Baseline Vs Optimized geometry (using FFD)

From the Cp distribution plots, it is quite evident that the shock regions were eliminated, resulting in smooth pressure distribution along the chord length of the optimized geometries. Both the parameterization techniques yielded almost similar geometries and pressure distribution. The results were achieved while using thirty-two design variables in the case of Hicks-Henne, whereas, in the case of FFD, six design variables (4 x 1 FFD box) were adequate. The values of these design variables were acquired after exploring the effect of the number of design variables on the optimized geometry.

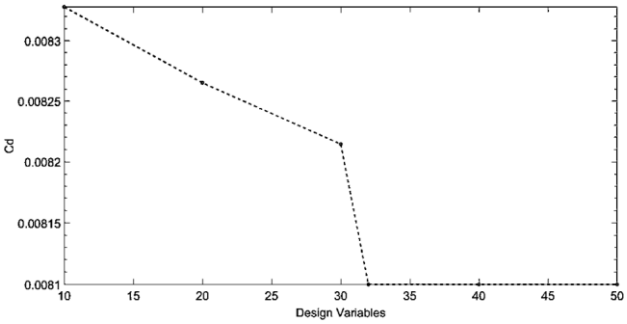

Figure 12: Effect of number of design variables on C_d(using HH)

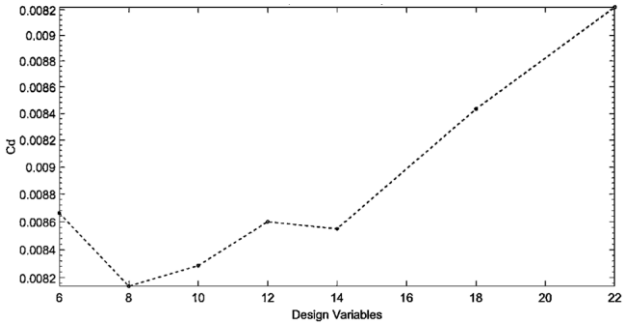

Figure 13: Effect of the number of design variables on C_d (using FFD)

Figure 12 and Figure 13 show the minimum number of design variables required for each parameterization to achieve the same optimized geometry. The number of design variables required for FFD is significantly lower than that for HH, making the FFD method more efficient.

The number of design iterations required to achieve the optimized geometry and satisfy the KKT conditions varied in both cases, as shown in Figure 14. The FFD method requires more design iterations to reach the same optimized geometry compared to the HH method, making the adjoint optimization based on FFD more computationally expensive.

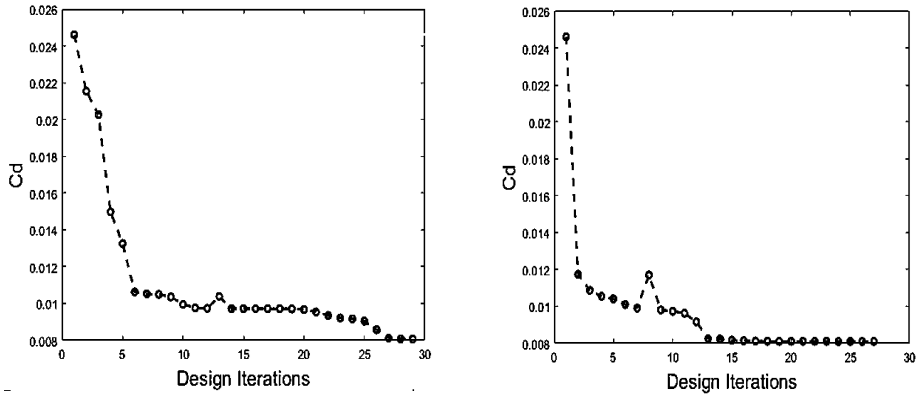

Figure 14: Design iteration required to reach the optimized shape using FFD (on left) and HH (on right)

Figure 15 shows the optimized airfoils achieved using both techniques, compared to the baseline. Although the optimized geometries largely overlap, a slight deviation near the trailing edge is observed. This deviation is attributed to the differences in the nature and properties of the parameterization methods.

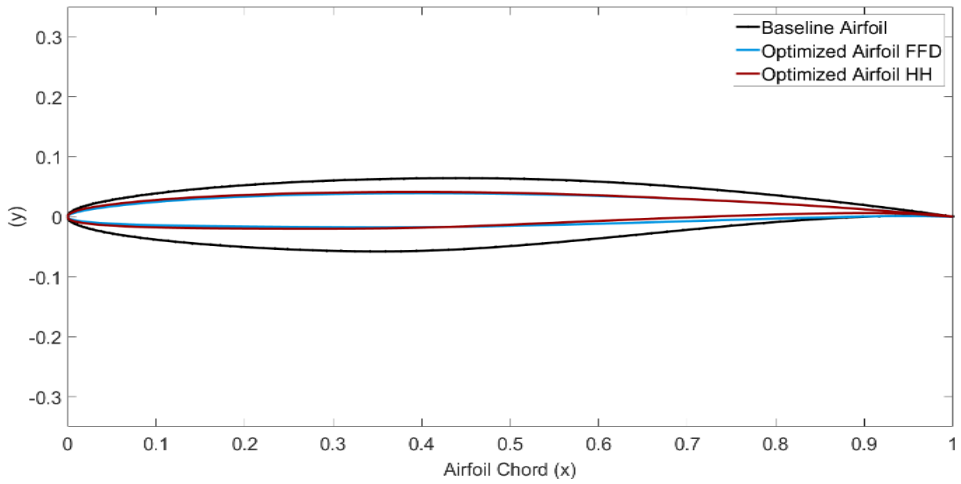

Figure 15: Comparison of baseline airfoil with optimized geometries (using FFD and HH)

Figure 16 presents the pressure, temperature, and Mach contours of the optimized geometries obtained using the Hicks-Henne and FFD parameterization techniques. Since the aerodynamic coefficients are similar, the contours appear identical. Additionally, it can be observed that there are no discontinuities or shocks on the surface of the optimized geometries.

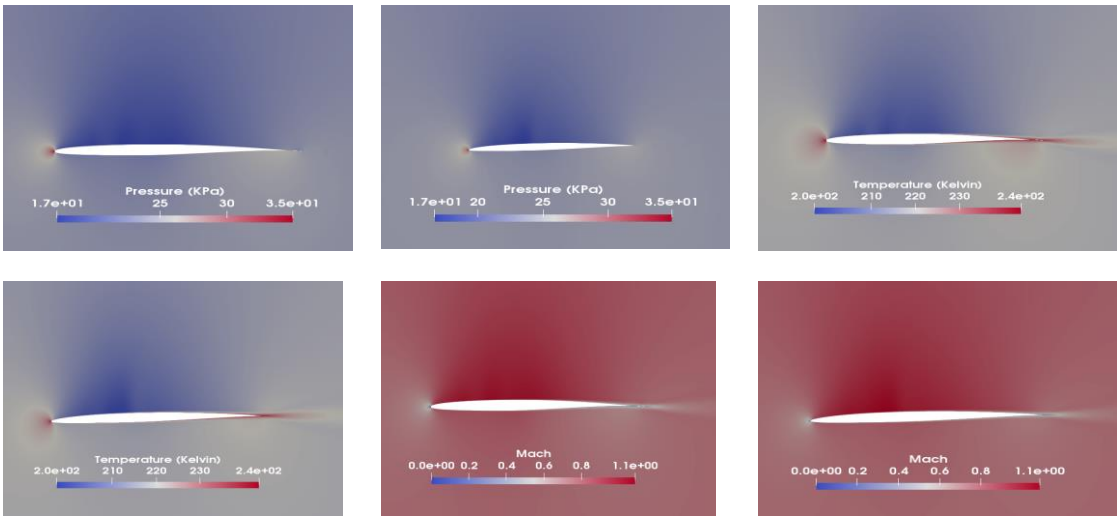

Figure 16: Pressure, Temp, and Mach Contours (HH geometry on left & FFD geometry-right)

The aerodynamic characteristics of the optimized geometries are summarized in table 6 as:

Table 6: Aerodynamic Characteristics of Optimized Geometry

Parameters	Values (HH Optimized)	Values (FFD Optimized)
Lift Coefficient C_l	0.3867	0.3867
Drag Coefficient C_d	0.0081	0.0080
Aerodynamic Efficiency	47.74	48.34
Airfoil Area	0.03838 m^2	0.03838 m^2

The optimization results indicate that both the Hicks-Henne and FFD techniques yielded geometries with aerodynamic properties that were nearly identical. However, a deeper analysis, based on the evaluation of fundamental characteristics, revealed that each technique displayed unique traits when compared and assessed quantitatively.

One of the primary metrics used to assess the efficiency of the techniques was parsimony, which refers to the number of design variables required to obtain the optimized geometry. In the case of the Hicks-Henne method, the optimal results were achieved using 32 design variables. In contrast, the FFD method reached its best results with just 8 control points. This significant difference highlights the relative efficiency of the FFD method, requiring only one-fourth of the design variables compared to Hicks-Henne. Based on this disparity, Hicks-Henne was awarded 1 point for parsimony, while FFD received the maximum score of 4 points, reflecting its higher efficiency in terms of the number of design variables needed for optimization.

Another key distinction between the two methods lies in the control they offer over the geometry. The FFD technique provides complete control over the geometry, enabling direct manipulation of the airfoil's geometric parameters. This direct control is particularly beneficial for shaping the airfoil with precision. In contrast, the Hicks-Henne method, by virtue of its formulation, restricts the placement of bumps at the leading and trailing edges of the geometry, limiting the degree of control over those critical regions. As such, Hicks-Henne indirectly controls the geometry, making it less intuitive than the FFD method. This characteristic led to FFD receiving the maximum score of 4 for intuitiveness, while Hicks-Henne was awarded 2 points. The greater flexibility and direct control of FFD make it a more intuitive choice for airfoil optimization.

Further, the optimization performance of both techniques was assessed by quantifying the number of design iterations required to converge on the optimized geometry. For Hicks-Henne, a sample of over 100 design iterations was generated, whereas FFD required over 350 geometries to explore the design space thoroughly. Each of these samples was carefully studied to assess the geometry and its features. A meticulous investigation revealed that no additional bumps, flaws, or intersecting flaws were present in any of the geometries produced by either method. This finding indicates that both techniques are capable of producing flawless geometries, and as such, both methods received the maximum score of 4 for flawlessness.

In terms of completeness, both techniques demonstrated the ability to approximate a wide range of airfoil shapes with a high degree of accuracy and tolerance. These shapes included the NACA 4 and 6 series, supercritical series, and other airfoil configurations, which are often encountered in aerodynamic design. Both methods were able to describe a significant number of airfoils, providing the optimizers with the ability to explore a large design space. Upon evaluating a total of 30 airfoil shapes, both Hicks-Henne and FFD produced a similar number of accurate approximations, resulting in each method receiving a maximum score of 4 for completeness. This shows that both methods are highly effective in covering the range of possible airfoil shapes with sufficient precision.

Regarding orthogonality, the assessment was based on established findings from the literature. In the Hicks-Henne method, sine bump functions are used as base functions, and these functions are inherently non-orthogonal. This lack of orthogonality leads to non-unique shapes being generated by different combinations of bump functions, making it difficult to predict the outcome of varying the parameters. Similarly, B-splines, which are employed by the FFD method, are also non-orthogonal in nature. As such, both methods were evaluated as having a non-orthogonal nature, leading to a score of zero in the orthogonality category. This characteristic is an inherent limitation of both parameterization methods, as they do not generate unique solutions from independent variables.

All the marks/points are summarized in table 7:

Table 7: Comparison Metrics

Techniques	Flawlessness	Completeness	Parsimony	Orthogonality	Intuitiveness
Hicks-Henne	4	4	1	0	2
FFD	4	4	4	0	4

As shown in Table 7figure, the FFD method achieved a total score of 16, reflecting its higher efficiency and intuitive control over the optimization process. In contrast, the Hicks-Henne method received a score of 11, indicating its relatively higher complexity in terms of the number of design variables and less intuitive control. The metrics provide valuable insights for designers when selecting a parameterization method, particularly within the class of deformable methods, for airfoil shape optimization. These comparison metrics can help guide decisions on the most appropriate method based on the specific goals of the design process, such as computational efficiency, control over the geometry, or the ability to explore a wide design space.

IV. CONCLUSION

This study presents a comparative analysis of two parameterization techniques—Hicks-Henne and Free-Form Deformation (FFD)—for adjoint-based shape optimization of the RAE-2822 airfoil at transonic Mach conditions. The optimization process led to significant aerodynamic improvements, including a 67% reduction in drag and a nearly threefold increase in aerodynamic efficiency. Despite both methods achieving similar aerodynamic performance, the comparison of their fundamental characteristics revealed clear differences in terms of efficiency and control over the geometry.

FFD demonstrated superior performance in several key areas. Specifically, it was found to be more parsimonious, requiring far fewer design variables to achieve the same optimized geometry. Additionally, FFD offered greater intuitiveness, providing direct and complete control over the airfoil's geometry, which made it more flexible and easier to manipulate compared to Hicks-Henne. On the other hand, Hicks-Henne, while effective in generating optimized geometries, proved less intuitive and required more design variables to reach the optimal result, making it computationally more expensive.

Both methods exhibited flawless geometries, with no significant flaws or defects found in the optimized shapes. Additionally, both techniques were capable of accurately approximating a wide range of airfoil shapes, demonstrating their completeness in covering a broad design space. However, the non-orthogonality inherent in both parameterization methods—due to the use of sine bumps in Hicks-Henne and B-splines in FFD—resulted in both methods receiving the same low score for orthogonality.

Overall, while both Hicks-Henne and FFD are effective for airfoil shape optimization, FFD is the more efficient and intuitive choice, particularly for applications requiring fewer design variables and greater control over the geometry. The findings of this study offer valuable insights into the strengths and limitations of each technique, providing guidance for future aerodynamic design and optimization tasks. The comparison metrics developed here will assist designers in selecting the most appropriate parameterization method for specific optimization goals, contributing to more efficient and effective shape optimization processes in aerodynamic applications.

CONFLICTS OF INTEREST

The authors declare that they have no conflicts of interest.

REFERENCES

[1] H. L. Silva et al., "A multidisciplinary design optimization for conceptual design of hybrid-electric aircraft," *Structural and Multidisciplinary Optimization*, vol. 64, no. 6, pp. 3505–3526, 2021. Available from: https://tinyurl.com/3sxt294v

[2] T. H. Ha, K. Lee, and J. T. Hwang, "Large-scale multidisciplinary optimization under uncertainty for electric vertical takeoff and landing aircraft," in *AIAA Scitech 2020 Forum*, 2020, p. 0904. Available from: https://doi.org/10.2514/6.2020-0904

[3] M. H. A. Madsen, F. Zahle, N. N. Sørensen, and J. R. R. A. Martins, "Multipoint high-fidelity CFD-based aerodynamic shape optimization of a 10 MW wind turbine," *Wind Energy Science*, vol. 4, no. 2, pp. 163–192, 2019. Available from: https://doi.org/10.5194/wes-4-163-2019

[4] S. Nasir, M. T. Javaid, M. U. Shahid, A. Raza, W. Siddiqui, and S. Salamat, "Applicability of Vortex Lattice Method and its Comparison with High Fidelity Tools," *Pakistan Journal of Engineering and Technology*, vol. 4, no. 1, pp. 207–211, 2021. Available from: https://doi.org/10.51846/vol4iss1pp207-211

[5] H. Koyuncuoglu and P. He, "CFD Based Multi-Component Aerodynamic Optimization for Wing Propeller Coupling," in *AIAA SciTech 2023 Forum*, 2023, p. 1844. Available from: https://doi.org/10.2514/6.2023-1844

[6] S. S. ul Hassan, M. T. Javaid, U. Rauf, S. Nasir, A. Shahzad, and S. Salamat, "Systematic investigation of power enhancement of Vertical Axis Wind Turbines using bio-inspired leading-edge tubercles," *Energy*, vol. 270, p. 126978, 2023. Available from: https://doi.org/10.1016/j.energy.2023.126978

[7] M. T. Javaid et al., "Power enhancement of vertical axis wind turbine using optimum trapped vortex cavity," *Energy*, vol. 278, p. 127808, 2023. Available from: https://doi.org/10.1016/j.energy.2023.127808

[8] J. Li, X. Du, and J. R. R. A. Martins, "Machine learning in aerodynamic shape optimization," *Progress in Aerospace Sciences*, vol. 134, p. 100849, 2022. Available from: https://doi.org/10.1016/j.paerosci.2022.100849

[9] J. Liu, R. Chen, J. Lou, Y. Hu, and Y. You, "Deep-learning-based aerodynamic shape optimization of rotor airfoils to suppress dynamic stall," *Aerospace Science and Technology*, vol. 133, p. 108089, 2023. Available from: https://doi.org/10.1016/j.ast.2022.108089

[10] P. Champasak et al., "Aircraft conceptual design using metaheuristic-based reliability optimisation," *Aerospace Science and Technology*, vol. 129, p. 107803, 2022. Available from: https://doi.org/10.1016/j.ast.2022.107803

[11] G. L. Halila, J. R. R. A. Martins, and K. J. Fidkowski, "Adjoint-based aerodynamic shape optimization including transition to turbulence effects," *Aerospace Science and Technology*, vol. 107, p. 106243, 2020. Available from: https://doi.org/10.1016/j.ast.2020.106243

[12] J. R. R. A. Martins, "Aerodynamic design optimization: Challenges and perspectives," *Computers & Fluids*, vol. 239, p. 105391, 2022. Available from: https://doi.org/10.1016/j.compfluid.2022.105391

[13] D. J. Poole, C. B. Allen, and T. Rendall, "Control point-based aerodynamic shape optimization applied to AIAA ADODG test cases," in *53rd AIAA Aerospace Sciences Meeting*, 2015, p. 1947. Available from: https://doi.org/10.2514/6.2015-1947

[14] D. Poole, C. Allen, and T. Rendall, "High-fidelity aerodynamic shape optimization using efficient orthogonal modal design variables with a constrained global optimizer," *Computers & Fluids*, vol. 143, pp. 1–15, 2017. Available from: https://doi.org/10.1016/j.compfluid.2016.12.009

[15] C. Lee, D. Koo, and D. W. Zingg, "Comparison of B-spline surface and free-form deformation geometry control for aerodynamic optimization," *AIAA Journal*, vol. 55, no. 1, pp. 228–240, 2017. Available from: https://doi.org/10.2514/1.J055102

[16] A. Jameson, "Aerodynamic design via control theory," *Journal of Scientific Computing*, vol. 3, no. 3, pp. 233–260, 1988. Available from: https://doi.org/10.1007/BF01061285

[17] A. Jameson and J. Reuther, "Control theory-based airfoil design using the Euler equations," in *5th Symposium on Multidisciplinary Analysis and Optimization*, 1994, p. 4272. Available from: https://doi.org/10.2514/6.1994-4272

[18] A. Jameson, L. Martinelli, and N. A. Pierce, "Optimum aerodynamic design using the Navier–Stokes equations," *Theoretical and Computational Fluid Dynamics*, vol. 10, no. 1, pp. 213–237, 1998. Available from: https://doi.org/10.1007/s001620050065

[19] R. Lei, J. Bai, and D. Xu, "Aerodynamic optimization of civil aircraft with wing-mounted engine jet based on adjoint method," *Aerospace Science and Technology*, vol. 93, p. 105285, 2019. Available from: https://doi.org/10.1016/j.ast.2019.07.018

[20] E. J. Nielsen and W. K. Anderson, "Aerodynamic design optimization on unstructured meshes using the Navier-Stokes equations," *AIAA Journal*, vol. 37, no. 11, pp. 1411–1419, 1999. Available from: https://doi.org/10.2514/2.654

[21] K. Telidetzki, L. Osusky, and D. W. Zingg, "Application of jetstream to a suite of aerodynamic shape optimization problems," in *52nd Aerospace Sciences Meeting*, 2014, p. 0571. Available from: https://doi.org/10.2514/6.2014-0571

[22] G. Carrier et al., "Gradient-based aerodynamic optimization with the elsA software," in *52nd Aerospace Sciences*

Meeting, 2014, p. 0568. Available from: https://doi.org/10.2514/6.2014-0568

[23] J. Reuther, A. Jameson, J. Farmer, L. Martinelli, and D. Saunders, "Aerodynamic shape optimization of complex aircraft configurations via an adjoint formulation," in *34th Aerospace Sciences Meeting and Exhibit*, 1996, p. 94. Available from: https://doi.org/10.2514/6.1996-94

[24] W. K. Anderson and V. Venkatakrishnan, "Aerodynamic design optimization on unstructured grids with a continuous adjoint formulation," *Computers & Fluids*, vol. 28, no. 4–5, pp. 443–480, 1999. Available from: https://doi.org/10.1016/S0045-7930(98)00043-7

[25] W. K. Anderson and D. L. Bonhaus, "Airfoil design on unstructured grids for turbulent flows," *AIAA Journal*, vol. 37, no. 2, pp. 185–191, 1999. Available from: https://doi.org/10.2514/2.689

[26] S. Nadarajah, "Aerodynamic design optimization: Drag minimization of the NACA 0012 in transonic inviscid flow,"

[27] Z. Lyu, G. K. Kenway, and J. R. Martins, "Aerodynamic shape optimization investigations of the common research model wing benchmark," *AIAA Journal*, vol. 53, no. 4, pp. 968–985, 2015. Available from: https://doi.org/10.2514/1.J053318

[28] G. K. Kenway and J. R. Martins, "Multipoint aerodynamic shape optimization investigations of the common research model wing," *AIAA Journal*, vol. 54, no. 1, pp. 113–128, 2016. Available from: https://doi.org/10.2514/1.J054154

[29] J. Elliott and J. Peraire, "Aerodynamic optimization on unstructured meshes with viscous effects," in *Computational Fluid Dynamics Review 1998: (In 2 Volumes)*, World Scientific, 1998, pp. 542–559. Available from: https://doi.org/10.1142/9789812812957_0030

[30] F. Palacios et al., "Stanford university unstructured (SU2): An open-source integrated computational environment for multi-physics simulation and design," in *51st AIAA Aerospace Sciences Meeting including the New Horizons Forum and Aerospace Exposition*, 2013, p. 287. Available from: https://doi.org/10.2514/6.2013-287

[31] Y. Shi, C. A. Mader, S. He, G. L. Halila, and J. R. Martins, "Natural laminar-flow airfoil optimization design using a discrete adjoint approach," *AIAA Journal*, vol. 58, no. 11, pp. 4702–4722, 2020. Available from: https://doi.org/10.2514/1.J058944

[32] M. Mangano and J. R. Martins, "Multipoint aerodynamic shape optimization for subsonic and supersonic regimes," *Journal of Aircraft*, vol. 58, no. 3, pp. 650–662, 2021. Available from: https://doi.org/10.2514/1.C036216

[33] X. He, J. Li, C. A. Mader, A. Yildirim, and J. R. Martins, "Robust aerodynamic shape optimization—from a circle to an airfoil," *Aerospace Science and Technology*, vol. 87, pp. 48–61, 2019. Available from: https://doi.org/10.1016/j.ast.2019.01.051

[34] Y. Shen, W. Huang, L. Yan, and T.-T. Zhang, "Constraint-based parameterization using FFD and multi-objective design optimization of a hypersonic vehicle," *Aerospace Science and Technology*, vol. 100, p. 105788, 2020. Available from: https://doi.org/10.1016/j.ast.2020.105788

[35] D. A. Masters, N. J. Taylor, T. Rendall, C. B. Allen, and D. J. Poole, "Geometric comparison of aerofoil shape parameterization methods," *AIAA Journal*, vol. 55, no. 5, pp. 1575–1589, 2017. Available from: https://doi.org/10.2514/1.J054943

[36] W. Chen and A. Ramamurthy, "Deep generative model for efficient 3D airfoil parameterization and generation," in *AIAA Scitech 2021 Forum*, 2021, p. 1690. Available from: https://doi.org/10.2514/6.2021-1690

[37] D. Anitha, G. Shamili, P. R. Kumar, and R. S. Vihar, "Airfoil shape optimization using CFD and parametrization methods," *Materials Today: Proceedings*, vol. 5, no. 2, pp. 5364–5373, 2018. Available from: https://doi.org/10.1016/j.matpr.2017.12.129

[38] V. Sripawadkul, M. Padulo, and M. Guenov, "A comparison of airfoil shape parameterization techniques for early design optimization," in *13th AIAA/ISSMO Multidisciplinary Analysis Optimization Conference*, 2010, p. 9050. Available from: https://doi.org/10.2514/6.2010-9050

[39] B. M. Kulfan, "The CST universal parametric geometry representation method, recent extensions and applications," in *Proc. R. Aeronaut. Soc. Conf.*, 2007, vol. 114, no. 1135, pp. 157–176. Available from: https://doi.org/10.2514/1.29958

[40] V. Braibant and C. Fleury, "Shape optimal design using B-splines," *Computer Methods in Applied Mechanics and Engineering*, vol. 44, no. 3, pp. 247–267, 1984. Available from: https://doi.org/10.1016/0045-7825(84)90132-4

[41] R. M. Hicks and P. A. Henne, "Wing design by numerical optimization," *Journal of Aircraft*, vol. 15, no. 7, pp. 407–412, 1978. Available from: https://doi.org/10.2514/3.58379

[42] J. A. Samareh, "Survey of shape parameterization techniques for high-fidelity multidisciplinary shape optimization," *AIAA Journal*, vol. 39, no. 5, pp. 877–884, 2001. Available from: https://doi.org/10.2514/2.1391

[43] T. W. Sederberg and S. R. Parry, "Free-form deformation of solid geometric models," in *Proceedings of the 13th Annual Conference on Computer Graphics and Interactive Techniques*, 1986, pp. 151–160. Available from: https://doi.org/10.1145/15922.15903

[44] S. Coquillart, "Extended free-form deformation: A sculpturing tool for 3D geometric modeling," in *Proceedings of the 17th Annual Conference on Computer Graphics and Interactive Techniques*, 1990, pp. 187–196. Available from: https://doi.org/10.1145/97879.97902

[45] L. T. Leifsson, S. Koziel, and S. Hosder, "Aerodynamic design optimization: physics-based surrogate approaches for airfoil and wing design," in *52nd Aerospace Sciences Meeting*, 2014, p. 0572. Available from: https://doi.org/10.2514/6.2014-0572

[46] O. Amoignon, J. Hradil, and J. Navratil, "Study of parameterizations in the project CEDESA," in *52nd Aerospace Sciences Meeting*, 2014, p. 0570. Available from: https://doi.org/10.2514/6.2014-0570

[47] J. Hradil, *Adaptive Parameterization for Aerodynamic Shape Optimization in Aeronautical Applications*, Brno University of Technology, Faculty of Mechanical Engineering, Institute of Aerospace Engineering, Brno, 2015.

[48] M. H. Sadraey, *Aircraft Design: A Systems Engineering Approach*. Hoboken, NJ, USA: John Wiley & Sons, 2012. Available from: https://doi.org/10.1002/9781118352700

[49] M. Ahmad, S. Nasir, Z. ur Rahman, S. Salamat, U. Sajjad, and A. Raza, "Experimental investigation of wing accuracy quantification using point cloud and surface deviation," *Pakistan Journal of Engineering and Technology*, vol. 4, no. 2, pp. 13–20, 2021. Available from: https://doi.org/10.51846/vol4iss2pp13-20